Proceedings of IMECE'02
2002 ASME International Mechanical Engineering Congress & Exposition
New Orleans, Louisiana, November 17-22, 2002

PERFORMANCE ANALYSIS OF BRAYTON AND RANKINE CYCLE MICROSYSTEMS FOR PORTABLE POWER GENERATION

Norbert Müller
Michigan State University
Dept. of Mechanical Engineering
2455 Engineering Building
East Lansing, Michigan 48824-1226
Phone: (517) 432 9139
Fax: (347) 412 7848
Email: mueller@egr.msu.edu

Luc G. Fréchette
Columbia University
Dept. of Mechanical Engineering
500 West 120th Street, 220 Mudd, MC4703
New York, New York, 10027
Phone: (212) 854-2962
Fax: (212) 854-3304
Email: lucf@alum.mit.edu

ABSTRACT

The presented work analyses the design space and performance potential of microfabricated Brayton cycle and Rankine cycle devices, accounting for lower component efficiencies, temperatures limited by the material properties and system implementation - constraints imposed by silicon microfabrication and miniaturization. By exploring the design space of such microsystems, their potential thermal efficiency and power density are defined. Results for both types of devices are shown graphically and design challenges and guidelines are determined and found to be different from their large-scale counterparts.

Similar analysis was performed for Brayton and Rankine cycle devices, with more complete assessment of the latter by including, windage, generator, conductive and heat sink losses. In contrast to the Brayton cycle, the compression work of the Rankine cycle is minimal and the pump efficiency is not critical. The investigation suggests a higher potential for Rankine cycle devices than for Brayton cycle devices.

Keywords: *Power MEMS, Microfabrication, Micro-turbine, Steam-turbine, Gas-turbine*

INTRODUCTION

The advent of microelectromechanical systems (MEMS) technology has opened the door to the creation of power systems at unprecedented small scales. Using microfabrication processes, it is suggested that common power generation systems could be miniaturized yielding high-power density, low-cost, batch manufactured power sources [1]. The implementation approach is however drastically different from traditional assembly of macro-scale components and introduces novel challenges in designing and integrating micro thermo-fluidic and electromechanical machinery. It consists of using MEMS fabrication technology, such as deep reactive ion etching of silicon (DRIE), wafer bonding, and thin film processing, to fabricate and integrate high speed rotating micro-turbomachinery, heat exchangers, and electromechanical machinery.

Initiated in 1995 [1], a growing effort has focused on developing the core technology for such microfabricated heat engines. While using silicon microfabrication technologies, the devices considered consist of millimeter-scale power plants [1,2,3]. They incorporate high speed rotating turbomachinery [4], an electromagnetic generator [5,6], fluid bearings [4,7], in some cases microchannel heat exchangers [8] and a combustor [9]. To date, these baseline components have been designed, microfabricated, and demonstrated specifically for a micro gas turbine generator and flight engine [1], micromotor-driven compressor [10], bi-propellant rocket engine with turbopumps [11].

Such small systems have the advantage of high power density, but at the cost of lower component efficiencies. Fundamentally, the specific work output of thermodynamic cycles is not a function of scale, but only of the fluid properties (temperature, pressure) at each point of the cycle. However, for constant performance levels the output power is proportional to the mass flow rate of working fluid through the device. As a device is reduced in size, the mass flow will scale as the through flow area, hence as the square of its characteristic

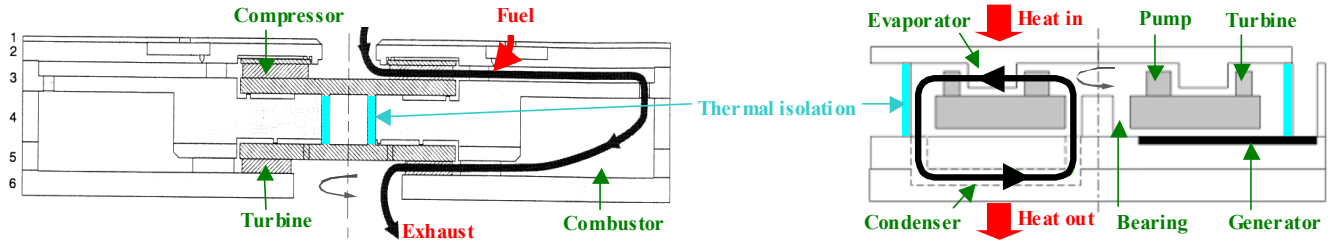

Figure 1:a) Brayton cycle device [1] (micro gas turbine engine) **b)** Proposed Rankine cycle device (micro steam-turbine)

dimension L. Since the mass or volume of the device will scale as the cubed of the characteristic length, its power density will increase as the device is miniaturized: Power/Mass=L^{-1}. Results for a micro rocket engine [11] and a microturbine [4] have demonstrated this dramatic increase in power density, referred to as the "cube-square law".

Miniaturization affects the ability and efficiency of the components to change the state of the working fluid. To date, miniature pumps, turbines, heat exchangers, and generators have not achieved the levels of performance (such as pressure ratio, for example) of their mature large-scale brethren. Current research efforts are bridging this gap [3], suggesting that it is mainly a question of time and engineering effort. Lower Reynolds numbers however characterize the fluid flow in miniature geometries, resulting in higher viscous losses and lower isentropic efficiency [12], effectively reducing their power density. Furthermore, the small-scale of these miniature devices induces high temperature gradients, which increases thermal losses and in turn impact the device performance. Analysis has shown that devices in the scale of hundreds of microns and above typically provide the appropriate trade-off between increased power density and reduced efficiency [12], although this scale is highly design dependant.

NOMENCLATURE

c_p	specific heat	J/kgK	η	efficiency
D	diameter	m	κ	isentropic exponent
Gap	gap	m	μ	friction coefficient
L	length	m	Π	pressure ratio
$\dot{m}$	mass flow	kg/s	τ	temperature ratio
P	power	Pa		
p	pressure	Pa	**Subcripts**	
q	specific heat flux	J/kg	1	turbine out
$\dot{Q}$	heat flow rate	W	2	compressor in
r	radius	m	3	compressor out
R	gas constant	J/kgK	4	turbine in
T	temperature	K	C	compressor
u	tip speed	m/s	f	friction
w	specific work	J/kg	Gap	with bearing loss
	dimensionless	-	max	maximum
X	bearing loss coefficient	-	min	minimum
			opt	optimum
β	flow angle	°	T	turbine
χ	swirl ratio	-	t	thermal

DEVICE DESCRIPTION AND FABRICATION

The overall dimensions of the considered devices are typically less than 3 mm thick x 1 cm^2. They can be fabricated using semiconductor and MEMS microfabrication processes. Single crystal silicon has been demonstrated as a viable material for high-performance micro-machinery. For example, DRIE and wafer bonded silicon structures have sustained high-speed rotation [4], high temperature gases in micro-combustors [9], and high pressures in rocket engines [11]. Furthermore, the integration of a thin film micromotor within a bonded wafer stack has been demonstrated [6], where axial and radial fluid-film bearings have supported the rotor, using the working fluid as a lubricant. The microfabrication approach limits the geometric design flexibility by the 2D nature of etching. Thus the turbomachinery cannot be truly three-dimensional. The etching essentially creates extruded-like blades from lithographically defined blade profiles. In the process first, the electrical components including the generator are fabricated on silicon wafers using thin film processing and lithography. Structures are then formed into the bulk of the silicon wafers by deep reactive ion etching (DRIE) of lithographically-defined features on both sides of the wafers. The flow paths are formed by fusion bonding the silicon wafers, creating a laminated, monolithic static structure that encloses a single crystal silicon rotor. This fabrication approach has successfully been demonstrated [4,6], but is still challenging for newer and advanced configurations required for complete systems.

Possible configurations of a Brayton cycle device and a Rankine cycle device are shown in Fig. 1. A significant difference between both is that the Brayton device features an open loop air cycle, whereas the Rankine device incorporates a closed loop allowing for different condensable working fluids; water is assumed in this work. Contrary to the Brayton device where the heat addition comes from the internal combustion in the combustion chamber and the heat is rejected with the exhaust gas, the Rankine device requires heat exchangers with the internal sides being the evaporator and condenser and the external sides being respectively the heat input (hot side) and heat sink for heat rejection (cold side). The external parts are not illustrated in Fig. 1b.

BRAYTON CYCLE DEVICE

This section investigates the design space of a microfabricated gas turbine to evaluate the potential net work output and efficiency, while accounting for characteristically low compressor efficiency. Adiabatic efficiencies on the order of 50-60% can be expected for adiabatic, low Reynolds number, planar compressors [13]. However, the short distance separating the compressor and turbine causes conduction and high levels of heat addition to the compressor flow path, effectively reducing its isentropic efficiency to values on the order of 30%. The following analyses investigate the impact of the isentropic compressor efficiency η_C on the overall efficiency η_t of a micro gas turbine, with and without bearing viscous losses. The cycle considered is a Brayton cycle (Fig. 2), with polytropic compression and expansion. The impact of heat addition in the compressor is captured by the low compressor efficiency. The temperature ratio τ and turbine efficiency η_T are assumed to be given.

The actual compressor specific shaft work w_C is determined by the compressor pressure ratio $\Pi = p_3/p_2$ and efficiency η_C.

$$w_C = \frac{c_p \cdot T_2}{\eta_C} \cdot \left(\Pi^{\frac{\kappa-1}{\kappa}} - 1 \right) \tag{1}$$

The corresponding temperature rise from the compressor inlet temperature T_2 to T_3 at the outlet is:

$$T_3 = T_2 + \frac{w_C}{c_p} \tag{2}$$

T_3 accounts for heat addition in the compressor, due to heat conduction from the turbine and combustor, by applying an adequate low η_C in Eq. 1. The necessary combustion heat per unit mass flow rate q results from the temperature difference between a fixed turbine inlet temperature T_4 and T_3.

$$q = c_p \cdot (T_4 - T_3) \tag{3}$$

The turbine specific shaft work is determined by Π and the turbine efficiency η_T. It is negative, since it is leaving the turbine.

$$w_T = \eta_T \cdot c_p \cdot T_4 \cdot \left(\Pi^{\frac{1-\kappa}{\kappa}} - 1 \right) \tag{4}$$

The engine overall efficiency η_t is defined positive, when the absolute value of the turbine shaft work is greater than the compressor shaft work needed.

$$\eta_t = \frac{-w_T - w_C}{q} \tag{5}$$

With Eq. 1 to 5 and defining the temperature ratio as $\tau = T_4/T_2$, the overall efficiency is determined by:

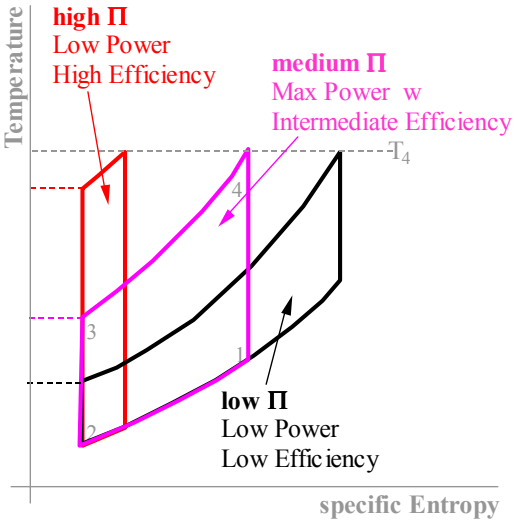

Figure 2: Brayton cycle

$$\eta_t = \frac{\eta_T \cdot \tau \cdot \left(1 - \Pi^{\frac{1-\kappa}{\kappa}} \right) + \frac{1}{\eta_C} \cdot \left(1 - \Pi^{\frac{\kappa-1}{\kappa}} \right)}{\tau - 1 + \frac{1}{\eta_C} \cdot \left(1 - \Pi^{\frac{\kappa-1}{\kappa}} \right)} \tag{6}$$

A dimensionless specific cycle work w is defined, that is positive when the engine performs work.

$$w = \frac{-w_T - w_C}{R \cdot T_2} \tag{7}$$

$$w = \frac{c_p}{R} \cdot \left(\eta_T \cdot \tau \cdot \left(1 - \Pi^{\frac{1-\kappa}{\kappa}} \right) + \frac{1}{\eta_C} \cdot \left(1 - \Pi^{\frac{\kappa-1}{\kappa}} \right) \right) \tag{8}$$

For a Brayton cycle (Fig. 2), it is well known that the cycle efficiency increases with the cycle pressure ratio and that there is an optimum pressure ratio for the maximum power density (Fig. 3). Again this becomes obvious with Fig. 2, being reminded that the enclosed area represents the cycle work.

Considering now the compressor efficiency η_C and turbine efficiency η_T for a cycle with polytropic compression and expansion, from Eq. 8 the optimum pressure ratio for maximum power density can be derived.

$$\Pi_{opt,w} = \left(\tau \cdot \eta_T \cdot \eta_C \right)^{\frac{\kappa}{2 \cdot (\kappa-1)}} \tag{9}$$

So, with $\eta_T<1$ and/or $\eta_C<1$ $\Pi_{opt,w}$ is always less than it would be in an ideal Brayton cycle with $\eta_T=\eta_C=1$ (Fig. 4). From Eq. 8 it also appears that for a fixed compressor efficiency $\eta_C<1$, there always exists an optimum pressure ratio $\Pi_{opt,\eta t}$ at which η_t is maximum, which is not the case in an ideal Brayton cycle with $\eta_T=\eta_C=1$. Generally: $\Pi_{opt,\eta t} > \Pi_{opt,w}$ (Fig. 4).

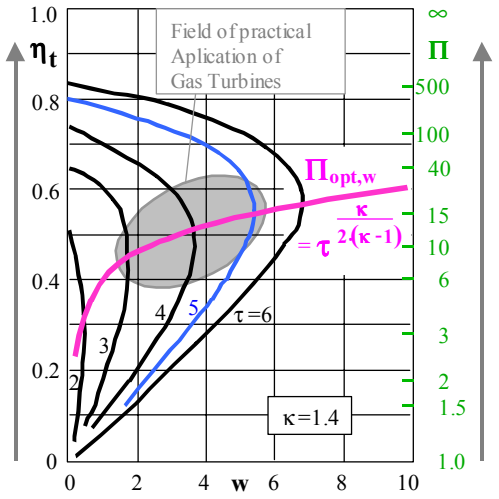

Figure 3: In an ideal Brayton cycle: an optimum pressure ratio for maximum power density exists and efficiency always increases with increasing pressure ratio

$$\Pi_{opt,\eta t}=\left(\frac{\eta_T\cdot\tau-\sqrt{\eta_T\cdot\eta_C\cdot\tau\cdot(1-\tau)\cdot\left(1-\tau\cdot(1-\eta_T)-\frac{1}{\eta_C}\right)}}{1-\tau\cdot(1-\eta_T)}\right)^{\frac{\kappa}{\kappa-1}} \quad (10)$$

For low compressor efficiency $\eta_C \approx 0.3\ldots0.5$ and low turbine efficiency $\eta_T \approx 0.5\ldots0.7$ the optima $\Pi_{opt,\eta t}$ and $\Pi_{opt,w}$ are relatively small and practically equivalent. For such low efficiencies $\Pi_{opt,\eta t}$ and $\Pi_{opt,w}$ mostly fall in the range of $\Pi_{opt} \approx 1.2\ldots5$. That differs significantly from the values for today's gas turbines, where $\Pi_{opt,\eta t}>30$ and $\Pi_{opt,w} \approx 10\ldots15$.

So, in contrast to the fact that increasing Π in today's normal scale gas turbines mostly leads to higher η_t, a relatively low pressure ratio Π can be preferable to obtain maximum engine efficiency η_t, or even necessary to close the cycle, in micro-fabricated gas turbines with low efficiencies (Fig. 5)

An additional characteristic of microfabricated turbomachinery is their planar nature, leading to a single stage, radial outflow compressor configuration. Achievable pressure ratio is therefore directly related to the tip speed , u_3. For that, a relation $\Pi(u_3)$ is needed. Assuming swirl free compressor inflow, from Euler's equation follows $w_C=u_3 \cdot c_{u3}$, where c_{u3} is the velocity component of the leaving fluid in circumferential direction. Furthermore, a swirl ratio at the compressor wheel exit is defined with $\chi_3=c_{u3}/u_3$, which can be seen as a dimensionless c_{u3}. By introducing the swirl ratio χ_3 instead of the more practical appearing exit flow angle β_3, the investigation becomes independent from the through flow component c_{m3} and thus no gas dynamic iteration is required to determine c_{m3} due to density change. A $\chi_3>1$ implies $c_{u3}>u_3$, which stands for forward sweep, $\chi_3<1$ stands for back sweep and $\chi_3=1$ stands for radial outflow. Eq. 1 can now be written:

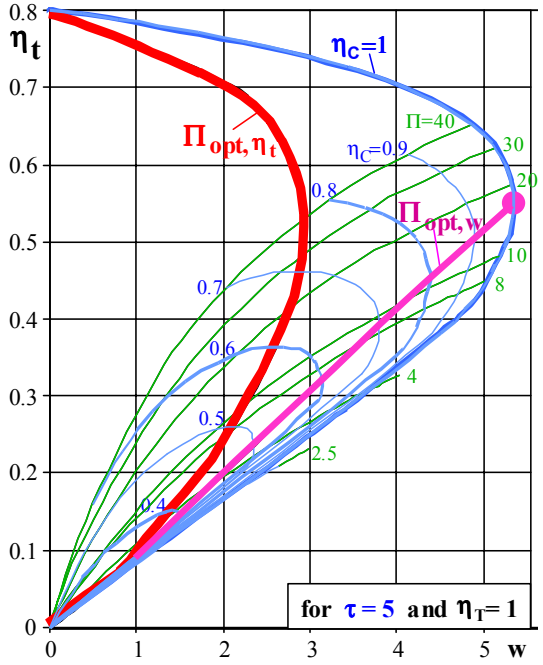

Figure 4: Comparison ideal Brayton cycle and Brayton cycle with $\eta_C<1$

$$u_3^2 \cdot \chi_3 = \frac{c_p \cdot T_2}{\eta_C} \cdot \left(\Pi^{\frac{\kappa-1}{\kappa}} - 1\right) \quad (11)$$

It appears that the u_3-curves are straight lines through the origin. The inclination of the u_3-lines is found by dividing Eq. 6 with Eq. 8. After substituting Π using Eq. 11, the relation $\eta_t(w,u_3)$ for constant u_3 is found:

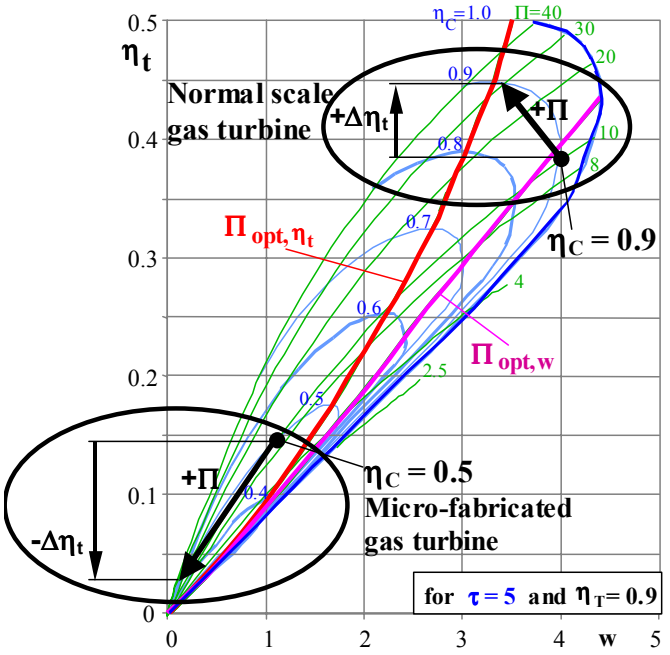

Figure 5: Comparison micro-fabricated gas turbine and normal scale gas turbine

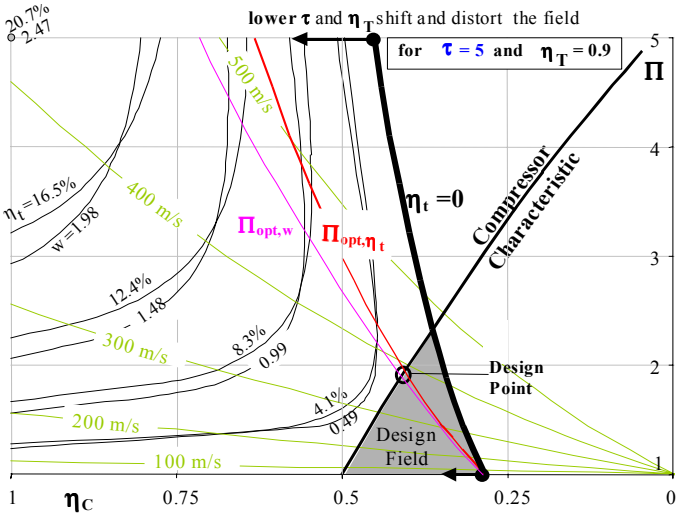

Figure 6: Design space for micro-fabricated gas turbines (u_3-curves for χ_3=1)

$$\eta_t = \frac{w \cdot R}{c_p \cdot (\tau - 1) + \frac{u_3^{\,2} \cdot \chi_3}{T_2}} \qquad (12)$$

Exactly the same relation will be found when bearing loss is considered using Eq. 16 and 19 instead of Eq. 6 and 8.

The plot in Fig. 5 is not very suitable to find the actual design space for a micro-fabricated gas turbine, but the inverse plot in Fig. 6 gives a much better picture of it. In Fig. 6 the u_3-curves distinguish very well from the other curves in the plot. They are determined by Eq. 11. Their inclination increases with χ_3, resulting in lower u_3 necessary for the same design point.

Figure 6 clearly shows the small design space for a micro-fabricated gas turbine and that low compressor efficiencies η_C clearly prohibit high Π. According to Fig. 6 the compressor pressure ratio is expected to be in the range of $\Pi \approx 1.5 \ldots 2.5$, not above. As indicated in Fig. 6 with lower τ and η_T, the line for the maximum pressure ratio $\Pi_{max}(\eta_C)$ where η_t=0 (Eq. 13), moves to the left decreasing the design space even more, while the compressor characteristic would stay the same.

$$\Pi_{max} = \left(\tau \cdot \eta_T \cdot \eta_C\right)^{\frac{\kappa}{\kappa - 1}} \qquad (13)$$

However, these low pressure ratios give much freedom to chose the combination of exit flow angle β_3 (or χ_3) and the circumferential velocity u_3. This design aspect is investigated next, along with the impact of bearing viscous drag.

Journal Bearing Loss

Since the previous section has shown that the maximum tip speed is not necessarily optimum, the tradeoff between circumferential velocity u_3 and exit flow angle β_3 in terms of χ_3

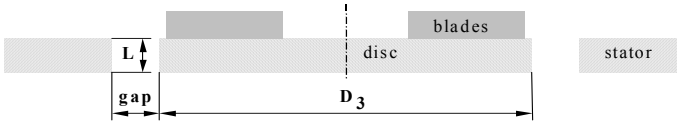

Figure 7: Journal bearing dimensions

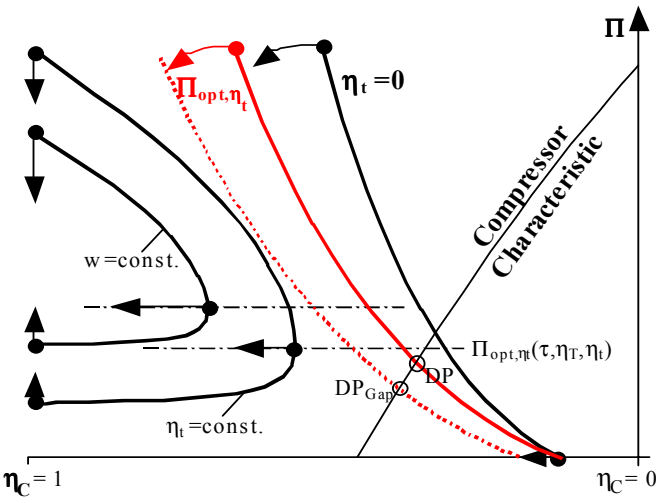

Figure 8: Shift and torsion of η_τ - and w-curve field with increasing X (schematically)

will be investigated next, while considering the journal bearing loss as a direct function of u_3. Typical dimensions of such a journal bearing (Fig. 7) are:

Rotor radius	r=D_3/2	=	4	mm,
Bearing length	L	=	400	µm,
Bearing gap	*gap*	=	15	µm.

In the bearing gap, Couette flow is assumed. Hence the shear stress is $\tau_f = \mu \cdot u_3 / gap$, with the dynamic viscosity of air $\mu \approx 2 \ldots 5 \cdot 10^{-5}$ kg/(m·s) for ≈300…1400K.

The power loss in the journal bearing P_f is the product of circumferential speed $\omega = u_3/r$ and torque $T = F \cdot r$, where F is the shear force $F = \tau_f \cdot A$ and A is the circumferential area $A = 2\pi \cdot r \cdot L$. This leads to a relation for the bearing loss with only practical design parameters:

$$P_f = 2\pi \cdot \mu \cdot u_3^{\,2} \cdot r \cdot \frac{L}{gap} \qquad (14)$$

Considering that the compressor shaft power is $P_C = w_C \cdot \dot{m}$, the turbine shaft power $P_T = w_T \cdot \dot{m}$, and the combustion heat rate $\dot{Q} = q \cdot \dot{m}$, with $\dot{m}$ being the mass flow rate, the engine overall efficiency in Eq. 5 becomes:

$$\eta_{t,Gap} = \frac{-P_T - P_C - P_f}{\dot{Q}} \qquad (15)$$

Using Eq. 14 and 11, Eq. 15 can be brought in the form:

$$\eta_{t,Gap} = \frac{\eta_T \cdot \tau \cdot \left(1 - \Pi^{\frac{1-\kappa}{\kappa}}\right) + \frac{1}{\eta_C} \cdot \left(1 - \Pi^{\frac{\kappa-1}{\kappa}}\right) \cdot (1 + X)}{\tau - 1 + \frac{1}{\eta_C} \cdot \left(1 - \Pi^{\frac{\kappa-1}{\kappa}}\right)} \qquad (16)$$

where X is a dimensionless loss coefficient of the journal bearing:

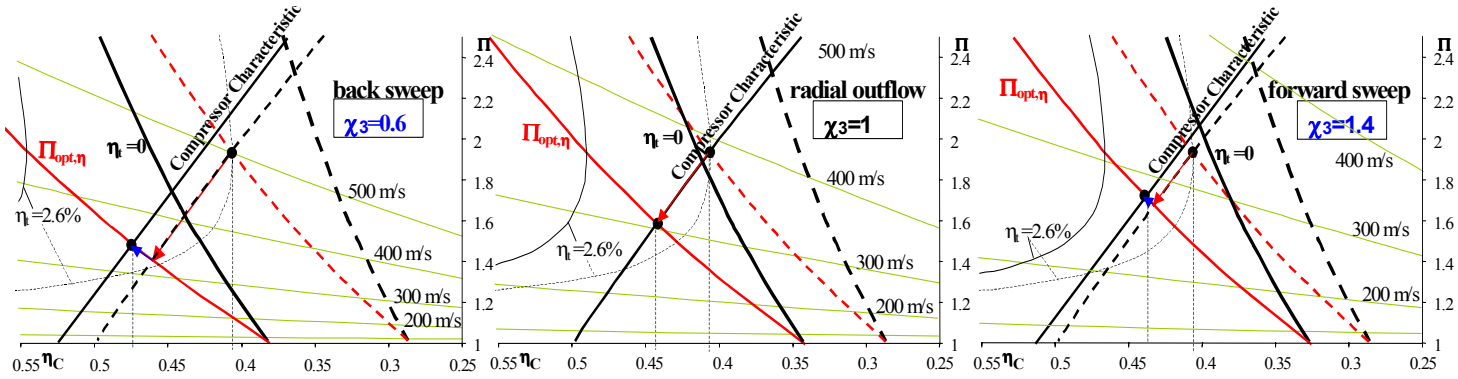

Figure 9: Design point shift for X>0 with different χ_3; τ=5 and η_T=0.7, D_3=8mm, L=400µm, gap=15µm, $\dot{m}$=0.1g/s, µ=3·10^{-5}kg/(m·s)

$$X = \frac{2\pi \cdot \mu \cdot r \cdot L}{\dot{m} \cdot \chi_3 \cdot gap} \tag{17}$$

Equation 17 again introduces only practical design parameters into Eq. 16. It shows that the bearing loss P_f is proportional to r, µ and L and inverse proportional to $\dot{m}$, χ_3 and gap.

While w_C, w_T and q are specific per unit mass flow, P_f is engine specific. Thus with higher mass flow $\dot{m}$ the specific bearing loss per unit mass flow decreases. Eq. 17 also shows that with forward sweep, the bearing loss is less than with back sweep, since a higher χ_3 lowers u_3 and in turn P_f.

Analogous to Eq. 7 and 8 the dimensionless specific cycle work w is now defined considering the bearing loss.

$$w_{Gap} = \frac{-P_T - P_C - P_f}{R \cdot T_2 \cdot \dot{m}} \tag{18}$$

$$w_{Gap} = \frac{c_p}{R} \cdot \left(\eta_T \cdot \tau \cdot \left(1 - \Pi^{\frac{1-\kappa}{\kappa}} \right) + \frac{1}{\eta_C} \cdot \left(1 - \Pi^{\frac{\kappa-1}{\kappa}} \right) \cdot (1+X) \right) \tag{19}$$

Eq. 9 modifies to:

$$\Pi_{opt,w,Gap} = \left(\frac{\tau \cdot \eta_T \cdot \eta_C}{1+X} \right)^{\frac{\kappa}{2\cdot(\kappa-1)}} \tag{20}$$

and Eq. 10 becomes:

$$\Pi_{opt,\eta t,Gap} = \left(\frac{\eta_T \cdot \tau - \sqrt{\eta_T \cdot \eta_C \cdot \tau \cdot (1-\tau) \cdot \left(1 - \tau \cdot (1-\eta_T) + (1-\tau) \cdot X - \frac{(1+X)}{\eta_C} \right)}}{1 - \tau \cdot (1-\eta_T) + (1-\tau) \cdot X} \right)^{\frac{\kappa}{\kappa-1}} \tag{21}$$

Figure 8 shows how the possible design space in Fig. 6 narrows due to the bearing losses. Keeping the design point at $\Pi_{opt,w}$, it moves from DP to DP_{Gap} along the compressor characteristic. Interesting values are summarized in Table 1.

In general, with greater X the field of η_t- and w-curves moves left, requiring a higher η_C for the same design point. With this shift, for constant η_t and w respectively $\Pi_{opt,w}(\tau,\eta_T,w)$ and $\Pi_{opt,\eta t}(\tau,\eta_T,\eta_t)$ (Eq. 22) stay constant, independent from X.

$$\Pi_{opt,\eta t}(\tau,\eta_T,\eta_t) = \left(\frac{\eta_T \cdot \tau + \sqrt{\eta_t \cdot \eta_T \cdot \tau \cdot (\tau-1)}}{\eta_T \cdot \tau - \eta_t \cdot (\tau-1)} \right)^{\frac{\kappa}{\kappa-1}} \tag{22}$$

Figure 9 shows enlarged views of the reduced design space with X>0 for different χ_3. Most significant is the decrease of u_3 when χ_3 increases. According to the general experience, simultaneously with the increase of χ_3 the compressor efficiency η_C decreases, due to the higher turning and exit flow velocity in the compressor wheel. This would be reflected in a down-shift of the compressor characteristic $\eta_C(\Pi)$. However, in the special case of a micro-fabricated engine with constant channel height, back sweep (χ_3<1) and forward sweep (χ_3>1) give the opportunity to narrow the flow channels toward the trailing edge accounting for the compression, which is hardly possible for radial outflow (χ_3=1), resulting in a η_C-penalty for radial outflow. Superimposing these effects is reflected in Fig. 9 by a strong up-shift of the compressor characteristic $\eta_C(\Pi)$ for back sweep and a slight up-shift for forward sweep, compared to the middle with radial outflow. This approach leads here to the same η_t for back and forward sweep and a lower η_t for radial outflow. Thus it appears from Fig. 9 that forward sweep is more favorable than back sweep to gain a higher η_t. The lower rpm connected with forward sweep also eases bearing stability requirements. This is concluded on the basis of the chosen configuration and $\eta_C(\Pi)$-characteristic. The decision will also be guided by practical design requirements and restrictions. So, a radial outlet might be preferred, for robust design considerations, but with lower η_t.

Table1: Design points (DP) for micro-fabricated gas turbines with and without bearing losses for χ_3=1, D_3=8mm, L=400µm, gap=15µm, $\dot{m}$=0.1g/s, µ=3·10^{5}kg/(m·s) (P_E…engine power)

Symbol	Π	η_C	P_T	P_C	P_f	P_E	Q	η_t	u_3	T_3
Unit	-	-	W	W	W	W	W	%	m/s	K
DP	1.940	0.406	-17.7	15.0	-	-2.7	102	2.60	388	443
DP_{Gap}	1.591	0.442	-12.7	9.4	1.89	-1.5	108	1.35	306	387

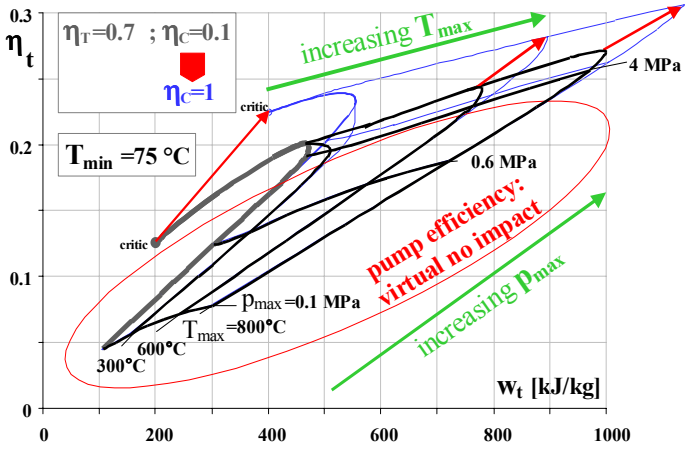

Figure 10: For a microfabricated Rankine cycle device pump efficiency has virtually no impact at thermal efficiency

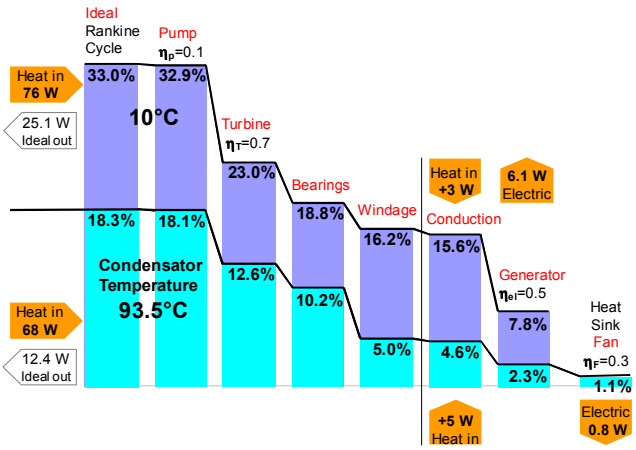

Figure 11: Predicted performance of a micro steam-turbine power plant-on-a-chip for aircraft (top bars) and standard application (lower bars)

Since the goal will be a compressor with as high efficiency as possible and producing an optimal pressure ratio, according to Eq. 10 or 16 respectively. This pressure ratio will typically be below 2.5, although it must be emphasized that no losses in the diffuser and combustor have been considered so far. Thus, the aimed pressure ratio of the compressor wheel may be higher than the investigations here suggest.

The compressor is clearly identified as the problematic part in a microfabricated Brayton device. Due to low compressor efficiency the design space is reduced to a minimum, where the work output of the turbine just exceeds the work used by the compressor. Despite cycle optimization, the overall cycle efficiency remains low, just enough to compete with battery systems. Additional electromechanical and combustion losses would further reduce the power output. An advantage however is the simplicity of the open loop device compared with a Rankine device and its potential use as propulsion for micro air vehicles.

RANKINE CYCLE DEVICE

An alternate approach for power generation based on micro heat engine technology would consist of a microfabricated Rankine cycle device, as proposed here. The main benefit stems from the relatively low compression power required. Additional challenges include phase-change flow-handling in a miniature closed loop, combined with the specific design of the internal and external high-flux heat exchangers.

The Rankine cycle considered here consists of (2→3) polytropic pressure rise of the liquid fluid coming from the condenser, (3→4) isobaric heat addition with phase change and superheating up to T_{max} in the evaporator, (4→1) polytropic expansion in the turbine and (1→2) isobaric heat rejection to fully condense the working fluid. Although supercooling is not considered here, it might be necessary to minimize cavitation in the pump.

Pump. The Rankine device suggests higher efficiency at microscale, since the problematic part of the Brayton cycle - the pressure rise - is achieved here by pumping the working fluid in its incompressible liquid state to the pressure p_{max}., minimizing the work required compared to a compressible gas. The pump uses a negligible fraction of the work supplied by the turbine. Especially in the relevant region of low and intermediate pressure rise, the pump efficiency is therefore not critical as shown in Fig. 10. A pump efficiency η_C of only 10% is assumed for the following analysis. However, the thermal efficiency η_t of the cycle rises considerably with the maximum pressure p_{max} achieved by the pump (Fig. 10).

Analyses. Since the Rankine cycle depends on phase change of the working fluid, the thermodynamic fluid properties vary drastically. Tabulated fluid properties or property correlations are therefore used, hindering an analytical approach to investigate the design field of a Rankine device. Hence only a numerical approach appears to be appropriate, and no formulas can be given for optimal design parameters. Instead, the investigation is performed by examples, which can always be optimized further in incremental steps depending on the specific application.

Examples. Two partly optimized examples are chosen here to evaluate the potential of a Rankine cycle device (Fig. 11). Both examples assume a device of dimension 1 cm^2 x 0.3 cm, and use a water flow rate of 24 mg/s, maximum temperature of 400°C and pump exit pressure of 0.6 MPa. One application consists of a typically ground-based portable power generation operating with still ambient air at 25°C, thus requiring an external cooling fan to remove heat from the condenser side. The second application consists of on-board aircraft power generation, rejecting heat to the atmosphere surrounding an aircraft at typical flight altitude, characterized by low temperatures and no need for a cooling fan. The analysis consisted of calculating the cycle performance, then subtracting the various losses from the turbine output power. The top bars in Fig. 11 represent the breakdown of power expenditure for the *aircraft application*. To prevent freezing of

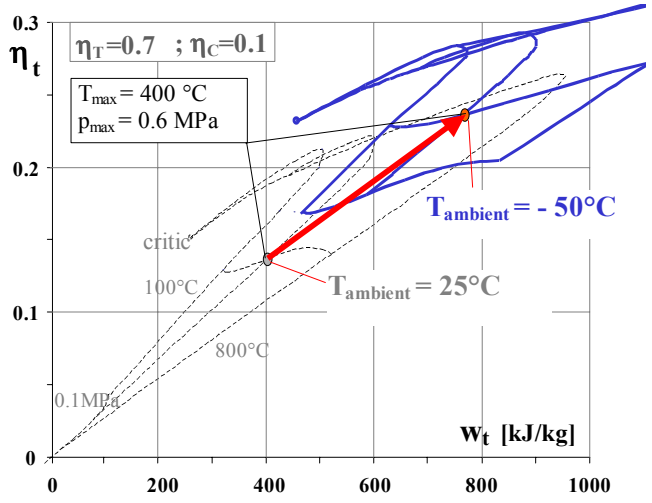

Figure 12: Increase of Rankine cycle efficiency and specific work with change of ambient temperature from 25°C to –50°C

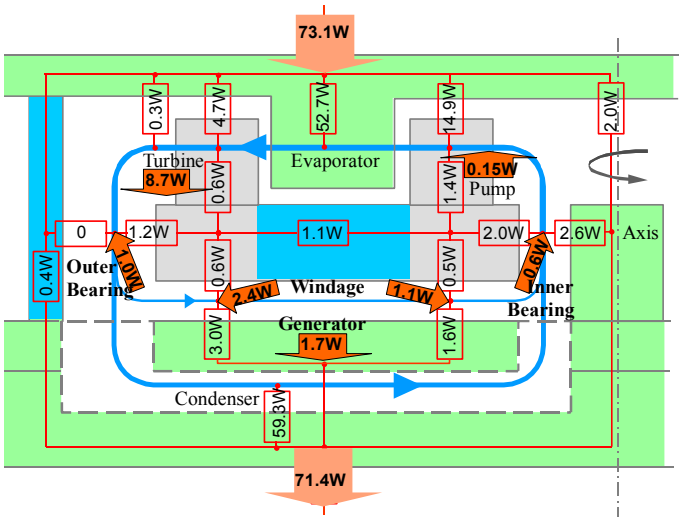

Figure 13: Thermal management and heat flow in Rankine cycle device for 25°C ambient temperature

the working fluid water, the condenser temperature is kept above 10°C. Using a working fluid with lower freezing point would allow a lower condenser temperature, higher efficiency, and increased output power. The output power is predicted to be on the order of 6W for a total heat input near 80 W, corresponding to an energy conversion efficiency of 7-8%. This includes bearing losses as well as losses due to disk windage, heat conduction and generator efficiency (50%), which were not considered for the Brayton cycle. Assuming a device density of 3g/cm^3, which is greater than that of silicon, an attractive power density of over 6kW/kg is obtained.

Also shown in Fig. 11 is the predicted performance of the *ground-based application* rejecting heat at usual ambient condition of 25°C air and using an external heat exchanger with cooling fan. System optimization suggests a condenser temperature of T_{min}=93.5°C, as a compromise between cycle power output and cooling fan power consumption. The ideal Rankine cycle efficiency suffers due to the higher T_{min} (Fig. 12). Accounting for the additional fan power expenditure, the output power decreases to 0.8 W and the overall efficiency to 1%. Both of these examples have the potential to be improved through optimization of the rotational speed, bearing and seal configuration, turbomachinery design, and device configuration. The superheated temperature and pump output pressure could also be increased beyond the conservative values adopted here.

In order to compare the Rankine and Brayton devices for similar levels of turbomachinery technology, the flow rate of the Rankine device was adjusted to the same through flow velocity component at the turbine exit of 150 m/s using a blade height of 400µm. Due to the lower fluid density the mass flow of the Rankine device is only around 1/4 of the Brayton device mass flow rate. The Rankine device is so predicted to output after bearing losses 14W and 7W for the aircraft and ground-based applications respectively, comparing favorably to 1.5 W of the same sized Brayton cycle device in Table 1.

Turbine. The pressure ratio of the turbine in a micro-fabricated Rankine device is much higher than in a Brayton device. The lowest density in the cycle occurs at the exit of the turbine, determining the maximum mass flow. Thus an outward flow turbine may be desirable to achieve a higher power density. The isentropic turbine efficiency was assumed to be η_T=0.7. With lower turbine efficiency the η_t-w_t map in Fig. 10 scales down to the origin, with practically no change in the overall shape. The isentropic turbine efficiency may increase with a configuration allowing for heat addition to the turbine.

Bearing. The general bearing configuration is similar to that of the Brayton device. Since the working fluid also acts as a lubricant, there is a choice between liquid or gas bearings in a Rankine device. Bearing losses are calculated according Eq. 14, where u_3 is taken to be the tangential velocity, u, at the journal bearing radius, r. The dynamic viscosity of water vapor for ≈300…500K is 1…2·10^{-5} kg/(m·s), approximately half that at the turbine outlet of a Brayton cycle with air. For water at ≈300K it is around twenty times more. Still the losses of a supporting bearing at the inner radius using water are about 3…5 times less then at the outer radius using water vapor, since the bearing loss is proportional to the radius cubed. Thus for higher efficiency a liquid bearing at the disc center is chosen. For the ground-based application with T_{min}=93.5°, there is a loss of 0.6W for the inner support bearing and additional 1W for the outer vapor backflow channel, acting as a secondary bearing with gap=30µm.

Windage. Additional disk windage is considered and calculated analogous to Eq. 14 with the rotational speed ω:

$$P_f = \frac{\pi}{2} \cdot \mu \cdot \omega^2 \cdot \frac{r_o^4 - r_i^4}{gap} \qquad (23)$$

for the outer part (turbine region, r_o=4mm, r_i=3mm) and the inner part (between pump inlet and turbine inlet, r_o=3mm,

r_i=1mm). For a gap=30μm, the disc windage sums up to 3.5W, where 2.4W are lost at the outer radii. Allowing water instead of steam in the disc gap would raise the windage up to 62W, clearly stating the need for proper seal and secondary flow design.

Thermal Management.

Beside the low power consumption of the pump, the second major advantage of the miniature Rankine cycle implementation compared to a Brayton cycle is the smaller maximum temperature difference in the device. Heat can however bypass the working fluid by conducting through the structure, increasing the heating and cooling load. Stray conduction is minimized by separating the hot and cold sides by a 700μm high silicon oxide cylinder with 25μm wall thickness and 8mm inner diameter. Heat transfer between the turbine and pump can be minimized by DRIE etching webs in the 300μm thick silicon rotor between the pump and the turbine, leaving 8 bridges of 2mm length, 200μm width. Figure 13 shows the thermal network modeling the thermal resistance of the structure. The heat flow through each resistor is calculated in an iterative process accounting for thermal transport in the fluid, the heat addition due to bearing and generator losses, windage and the work transmission in pump and turbine as well as the extracted electrical energy. The energy available to the generator is 3.4W (= +Turbine –Pump – Windage –Bearing losses). The 50% effective generator produces 1.7W electrical energy and feeds 1.7W heat back in the structure.

Figure 13 shows that ≈15W, or about 25% of the heat supplied to the cycle, is added in the pump, requiring measures preventing excessive cavitation in the pump. These could consist of supercooling the fluid and thermal isolation of the outer pump shroud from the heat source.

Condenser. The internal condenser is cooled by an external heat sink with a base area of 1 cm^2. The external heat sink design must be optimized to maximize the heat transfer and minimize power demand for the cooling fluid, as described elsewhere [8]. If forced convection is not provided by other means, such as the airflow around an aircraft or other vehicle, a fan is needed to force the cooling air through the heat sink, For the ground-based example with 25°C ambient air and using a 30% efficient fan, a heat sink configuration demanding 0.9W fan power can be found [8].

Evaporator. The evaporator consists of an external part collecting heat from a heat source (hot side) and internal fins or microchannels, which can potentially protrude in the flow path between the pump and turbine or be located above the turbomachinery. High velocities through microchannels or fins promote large heat transfer rates, vaporizing the flow before entering the turbine. Compensating for pressure losses through the heat exchangers, the additional pressure rise required from the pump is traded against the achievable high heat transfer rates, which may be viable since the pump performance plays a minimal effect on a Rankine cycle efficiency. For superheating, care may be taken to separate the superheater from the evaporator to achieve stable boiling in the evaporator and account for the large specific volume increase upon phase change. Superheating is necessary to minimize or prevent two-phase flow in the turbine. Superheating does not increase the cycle efficiency linearly; depending on the chosen cycle parameters, there may be an optimum as Fig. 12 shows.

Heat Source. Two types of heat sources are envisioned: (1) dedicated combustor integrated in or closely attached to the device, (2) waste heat brought in the chip by convection or conduction. From a system level perspective, harvesting electricity from waste heat can create additional pressure loss in the source flow or add a thermal resistance on the source, which can cause an undesirable rise of its temperature.

The maximum cycle temperature can be as high as the material can sustain. For pressurized or rotating parts, material creep has to be prevented, hence limiting temperature of silicon to <900°C. An integrated combustor would probably be the hottest heat source. In this analysis, the maximum fluid temperature used was 400°C, allowing a conservative margin in the performance and efficiency predictions. Waste heat from a flow for example can be harvested from a large-scale jet engine or a microfabricated Brayton cycle device, using the Rankine device as a bottom cycle device. For the latter, the current assessment suggests that the Rankine cycle would provide the larger fraction of energy, effectively increasing the power output and efficiency of either cycle operating independently. Waste heat may also be harvested from hot engine structures, power electronics or microprocessors. Solar heat sources providing high temperatures through the use of collecting mirrors or lenses are also envisioned for applications such as distributed environmental sensors or on-board spacecraft.

CONCLUSION

Microfabricated Brayton and Rankine cycle devices can serve as distributed power generation systems, with low efficiencies (in the range of 1-10%) but high power density. The main problem of the microfabricated Brayton cycle device is low compression efficiency due to the microfabrication approach and to the high heat conduction from the turbine to the compressor, a result of miniaturization. Still the microfabricated Brayton device is a relative simple open loop device without any heat exchangers.

The Rankine cycle device benefits greatly from the low power consumption of the pump. The internal temperature differences are much less, hence allowing a thermal management with low conductive heat losses. Further, the Rankine cycle device features a closed loop, permitting the use of working fluids adapted to certain applications. The presence of the liquid fluid in a Rankine cycle enables the use of pressurized liquid journal bearings, featuring potentially advantageous bearing stiffness. Two-phase flow management and stable phase change and superheating in integrated micro high-flux heat exchangers are expected to be significant practical challenges.

The small scale power components differ mainly from their large scale brethren in their *higher power density* but *lower efficiency*. Design constraints and guidelines are different from the large-scale counterparts too. For the microfabricated Brayton cycle device it was found that the low compression efficiency reduces the possible design space to relatively low pressure ratios of 1.5…5. This gives some freedom in the choice of the compressor outlet flow angle. Forward sweep combined with lower tip speed was found to have probably the best potential to obtain satisfying system efficiencies. In the small design space for the microfabricated Brayton device, the pressure ratio optimum for highest efficiency lays very close to the optimum for maximum power density (net work output).

It was found that the Rankine cycle micro power generation system is more promising in terms of thermal efficiency and power density than the Brayton cycle, especially if disc windage, bearing, generator, conductive and heat sink losses are included in the analysis.

Increased power output can be achieved by using more devices in parallel, covering larger areas. Due to the planar shape of the devices, laying out arrays of power plant chips can form power-generating sheets. Providing high geometric flexibility, these sheets can be closely integrated with current and future airframes, propulsion systems or adapt to practically any form factor of possible heat sources. Due to the small size of each power-generating device, the technology is directly scalable for heat sources of all sizes in vehicular or stationary applications. In addition, the devices can be distributed throughout a system, for local power generation and energy scavenging. This is a radical departure from the current centralized power generation, which leads to attractive benefits, like improved reliability due to the high redundancy. The distributed nature will also limit the impact of localized failures or damage. Distributed information processing has emerged from the advent of integrated circuits and the microprocessor, and similarly, distributed energy conversion will lead to new integrating concepts for power generating systems.

The microfabrication approach lends itself well to batch processing, as demonstrated by the semiconductor industry. Hundred of power plants-on-a-chip can be manufactured in parallel from silicon wafers using optical lithography and etching processes. When produced in large quantities, devices of high complexity can be produced at low unit cost. The microfabrication approach also opens the path for integrated electronic circuitry and power electronics, with limited added cost.

Overall, this work defines the plausible design space and identifies design constraints and guidelines for the future development of power-plant-on-a-chip microsystems for stationary or portable power generation. Challenges were identified in component efficiencies of compressor and turbine, thermal isolation, and two-phase flow in a Rankine cycle.

REFERENCES

[1] Epstein A.H. et al., 1997, “Micro-Heat Engines, Gas Turbines, and Rocket Engines – The MIT Microengine Project”, AIAA Paper 97-1773, *28th AIAA Fluid Dynamics Conference*, Snowmass Village, CO.

[2] Epstein A.H., 1997, and Senturia S.D., “Macro Power from Micro Machinery”, Science, **276**, p.1211.

[3] Epstein A.H, Jacobson S.A., Protz J., Fréchette L.G., 2000, "Shirtbutton-Sized Gas Turbines: The Engineering Challenges of Micro High Speed Rotating Machinery". *Proc. 8th International Symposium on Transport Phenomena and Dynamics of Rotating Machinery*, Honolulu, Hawaii.

[4] Fréchette L.G. et al., 2000, “Demonstration of a Microfabricated High-Speed Turbine Supported on Gas Bearings,” *Proc. Solid-State Sensor and Actuator Workshop*, Hilton Head Is. NC.

[5] Nagle S.F., and Lang J.H., 1999, “A Micro-Scale Electric-Induction Machine for a Micro Gas Turbine Generator” *27th Annual Meeting of the Electrostatics Society of America*.

[6] Fréchette, L.G. et al., 2001, "An Electrostatic Induction Micromotor Supported on Gas-Lubricated Bearings". *Proc. 14th IEEE Int’l Conf. on Micro Electro Mechanical Systems*, Interlaken, Switzerland, pp. 290-293.

[7] Piekos E. S. et al., 1997, "Design and Analysis of Microfabricated High Speed Gas Journal Bearings", AIAA paper 97-1966, *28th AIAA Fluid Dynamics Conference*.

[8] Müller N. and Fréchette L.G., 2002, “Optimization and Design guidelines for high flux Micro-Channel heat Sinks for liquid and gaseous single-phase flow”, *Proc. 8th Inter Society Conference on Thermal and Thermomechanical Phenomena in Electronic Systems (ITHERM 2002)*, San Diego, CA, pp 449-456.

[9] Mehra A. et al., 2000, “A six-wafer combustion system for a silicon micro gas turbine engine”, *Journal of MEMS*, **9**, No. 4., pp. 517-527.

[10] Fréchette, L.G., 2000, “Development of a microfabricated silicon motor-driven compression system“, Ph.D. Thesis, Massachusetts Institute of Technology.

[11] London A.P., Epstein A.H., Kerrebrock J.L., 2001, “High-Pressure Bipropellant Microrocket Engine”, AIAA J. of Propulsion and Power, **17**, No. 4, pp. 780-787.

[12] Jacobson S. A., 1998, “Aerothermal Challenges in the Design of a Microfabricated Gas Turbine Engine”, *AIAA 98-2445, 29th Fluid Dynamics Conference*, Albuquerque, NM.

[13] Mehra, A., 1997, “Computational Investigations and Design of Low Reynolds Number Micro-Turbomachinery”, M.S. Thesis, Massachusetts Institute of Technology.